

DOI: 10.1002/cssc.201100798

Design of a Highly Nanodispersed Pd–MgO/SiO₂ Composite Catalyst with Multifunctional Activity for CH₄ Reforming

Hyun You Kim,^[b] Jung-Nam Park,^{*[a]} Graeme Henkelman,^[b] and Ji Man Kim^[a]

We describe a highly nanodispersed Pd–MgO/SiO₂ composite catalyst synthesized by an in situ, one-pot, reverse microemulsion method as a multifunctional catalyst for low-temperature CH₄ reforming. Experimental results suggested evidence for a synergistic interplay of each component and DFT calculations confirmed a multifunctional reaction mechanism of CH₄ reforming and the importance of the Pd–MgO interface. We find

that the Pd nanoparticle binds and dissociates CH₄, that MgO activates CO₂ and increases coking resistance, and that SiO₂ prevents Pd sintering. CO spillover from Pd to MgO opens a faster pathway for CO production. A unique and groundbreaking feature of the present catalyst is the well-designed cooperation of each element that assures long-lasting, consistent, high- and low-temperature activity.

Introduction

Increasing atmospheric concentrations of greenhouse gases, primarily associated with fossil-fuel combustion, is creating a critical risk for the earth's climate system.^[1,2] Turning to clean energy sources, such as solar energy, nuclear fusion, or hydrogen, will eventually solve the issues raised by greenhouse gas emissions. Despite efforts towards the development and application of sustainable and renewable energy sources, the energy required for transportation and electricity is still mostly supplied by petroleum and coal combustion, which emits substantial amounts of CO₂—the most critical greenhouse gas.^[3] Several utilization technologies for CO₂, such as CO₂ capture, storage or sequestration, and chemical conversion, are becoming key issues in recent efforts to reduce the atmospheric concentration of CO₂.^[2–5] In this context, the utilization of greenhouse gases as a feedstock in chemical processes for the synthesis of fuels or valuable products, regarding them as an energy carrier, could be highly effective at minimizing future greenhouse gas emissions.^[3,5,6]

The reforming of CH₄ has been regarded as an initial step in the conversion of natural gas feedstock into viable energy sources, namely, hydrogen and synthetic gas (syngas; CO + H₂).^[6,7] Valuable hydrocarbon chemicals can then be obtained from syngas by subsequent Fisher–Tropsch (FT) synthesis.^[7–9] Moreover, utilizing two of the most critical greenhouse gases, CO₂ and CH₄, CH₄ reforming is attracting interest as an eco-friendly reaction that can reduce the risk of greenhouse gases towards climate change.^[1,7]

Dry reforming (DR; CH₄ + CO₂ → 2CO + 2H₂) and steam reforming (SR; CH₄ + H₂O → CO + 3H₂) of CH₄ are performed with transition-metal catalysts.^[9,10] Catalyst deactivation phenomena by carbonaceous deposition on the active site, coking, and agglomeration of metal catalysts have been critical issues in CH₄ reforming employing metal nanoparticles.^[6,11] Although noble-metal catalysts show higher carbon resistance than early-transition-metal catalysts,^[12,13] they are still prone to deactivation by

agglomeration. Additionally, the low catalytic activity of conventional catalysts at low temperatures (<450 °C), originating from a high reaction energy barrier, has to be improved to efficiently utilize CH₄ and CO₂ with a combination of subsequent FT synthesis.


In this study, we designed and synthesized a Pd–MgO/SiO₂ composite catalyst with a state-of-the-art, simple, one-pot, reverse microemulsion (ME) method and tested it as a new catalyst for CH₄ reforming. The one-pot reverse ME method, including hydrolysis and condensation of porous silica, enables in situ synthesis of nanocomposite catalysts. The catalyst was carefully designed on the basis of the bifunctional catalysis concept and previous findings on SiO₂-encapsulated catalysts.

A bifunctional catalyst, composed of two or more active components, is regarded as a composite heterogeneous catalyst that can activate complicated chemical reactions.^[14–16] Each component of the bifunctional catalyst facilitates a specific part of the reaction, leading to more efficient reaction pathways without competition between reactants for a single reaction site and poisoning of active sites.

In a previous report, we found that Pd/SiO₂ modified with additional MgO catalyzed CO₂ methanation with higher CO₂ conversion and CH₄ selectivity.^[15,16] MgO strongly binds CO₂ by

[a] Dr. J.-N. Park, Prof. J. M. Kim
Department of Chemistry, BK21 School of Chemical Materials Science
and Department of Energy Science
Sungkyunkwan University, Suwon, 440-746 (Republic of Korea)
Fax: (+82) 512-471-6835
E-mail: pjungnam@gmail.com

[b] Dr. H. Y. Kim, Prof. G. Henkelman
Department of Chemistry and Biochemistry
University of Texas at Austin
1 University Station A5300 Austin
Texas, 78712-0165 (USA)

 Supporting Information for this article is available on the WWW under <http://dx.doi.org/10.1002/cssc.201100798>.

forming an Mg–CO₃ carbonate species, whereas Pd nanoparticles bind and dissociate H₂, supplying hydrogen for hydrogenation of CO₂ on MgO. We, therefore, have chosen the MgO modifier to separate the reaction pathway of CH₄ reforming into two parts: dissociative adsorption of CH₄ on Pd nanoparticles and CO₂ adsorption and activation on MgO. We speculate that reactions on Pd would proceed more efficiently because MgO takes the CO₂-related portion of the reaction. Our previous studies have shown that when Pd nanoparticles, prepared by a reverse ME method, are encapsulated in a gas-permeable porous SiO₂ shell, they possess excellent sinter resistance without a decline in catalytic activity.^[17,18] From an industrial perspective, this is a highly promising result because the catalyst is essentially free from deactivation by sintering. We have applied a SiO₂ encapsulation method to our catalyst.

To investigate the effects of the SiO₂ shell and MgO content on the catalytic properties, we synthesized Pd–MgO/SiO₂(ME) catalysts with various initial Mg loadings (0–6.8 wt%) through a reverse ME method and two control group catalysts prepared with a conventional impregnation (Imp) method, Pd/SiO₂(Imp) and Pd–MgO/SiO₂(Imp).

Our results indicate that MgO dramatically improves catalytic activity and SiO₂ enhances the structural stability of the catalyst. Both results improve resistance to catalyst deactivation. Mechanistic studies performed by using DFT confirm the multifunctional reaction mechanism, synergistic interplay of Pd and MgO, and the simultaneous operation of DR and SR of CH₄ for the first time.

The results presented herein describe a new catalyst for the chemical conversion of greenhouse gases into hydrogen and valuable chemicals as well as a design scheme for advanced catalysts for the chemical conversion of greenhouse gases and complicated multistep reactions.

Results and Discussion

Catalytic properties of Pd–MgO/SiO₂(ME)

The morphologies of the Pd–MgO/SiO₂(ME) and Pd–MgO/SiO₂(Imp) catalysts as-synthesized and after the CH₄ reforming reaction are shown in Figure 1. Features within the image of the as-synthesized Pd–MgO/SiO₂(ME) (Figure 1a) are consistent with the remnants of silica shells surrounding the electron-dense centers, identified as Pd and Mg.^[16] The particles appear to be uniform in shape with a diameter of (5.5 ± 2.0) nm. The apparent frog-spawn-like morphology was preserved, even after 15 h of reaction at 700 °C, without any significant agglomeration of the Pd nanoparticles (Figure 1c). Because the Pd nanoparticles in as-synthesized Pd–MgO/SiO₂(Imp) grew into large crystallites after the reaction (Figure 1b and d), the sinter resistance of Pd–MgO/SiO₂(ME) originates primarily from the SiO₂ encapsulant.

XRD data shown in Figure 2 show that the SiO₂ encapsulant of the current catalysts synthesized by the ME method is non-crystalline and amorphous. We did not find any XRD peak that fit to a crystalline SiO₂ phase. Higher BET surface areas and N₂ adsorption–desorption isotherms of catalysts synthesized by

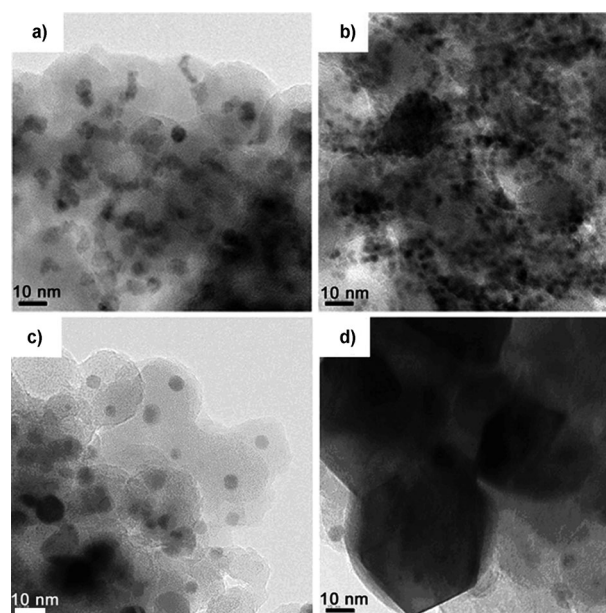


Figure 1. Sinter resistance of the Pd–MgO/SiO₂(ME) catalyst. The SiO₂ shell prevents agglomeration of the Pd nanoparticles. TEM images of a) Pd–MgO/SiO₂(ME) and b) Pd–MgO/SiO₂(Imp). TEM images of catalysts c) Pd–MgO/SiO₂(ME) and d) Pd–MgO/SiO₂(Imp) exposed to CO₂ and CH₄ for 15 h at 700 °C.

the ME method confirmed that the SiO₂ layer was porous and thus gas permeable (Table S1 and Figure S1 in the Supporting Information). XRD data also show that the Pd phase of as-synthesized catalysts is mainly PdO, which was later reduced to a Pd metal phase after CH₄ reforming (Figure 2). X-ray photoelectron spectra of Pd3d_{5/2} confirmed that most of the Pd²⁺ [binding energy (B.E.) = 338.7 eV] and Pd⁺ (B.E. = 336.9 eV) ions were reduced to Pd⁰ (B.E. = 335.4 eV) after the reaction (Figure S2 in the Supporting Information). Because such reduction of the PdO_x phase was observed in other reactions,^[16,17] we believe that even though PdO_x phases are present in as-synthesized catalysts, they do not play a critical role in the reaction mechanism of CH₄ reforming.

The temperature-programmed reaction results shown in Figure 3 and the CH₄ conversion and CH₄ reaction rates for the catalysts studied at 450 and 700 °C presented in Table 1 show that the MgO and SiO₂ encapsulant dramatically improves the catalytic properties of the Pd nanoparticles. Figure 3 shows that the initial CO and H₂ production of Pd nanoparticles encapsulated in the SiO₂ shell, Pd/SiO₂(ME), is approximately 40% higher than that of Pd/SiO₂(Imp). The results show that the catalytic activity of Pd/SiO₂(Imp) rapidly decreased and completely declined after 4.5 h (the experiments could not be continued due to gas blockage caused by severe sintering after 4.5 h). We also observed severe Pd agglomeration in the Pd/SiO₂(Imp) catalyst, even from early stages of the reaction. Because Pd agglomeration was not observed in Pd/SiO₂(ME), it is clear that the SiO₂ encapsulant prevents catalyst agglomeration and corresponding deactivation.

Although the SiO₂ shell prevents Pd agglomeration and rapid decline in catalytic activity of the Pd nanoparticle, the CO

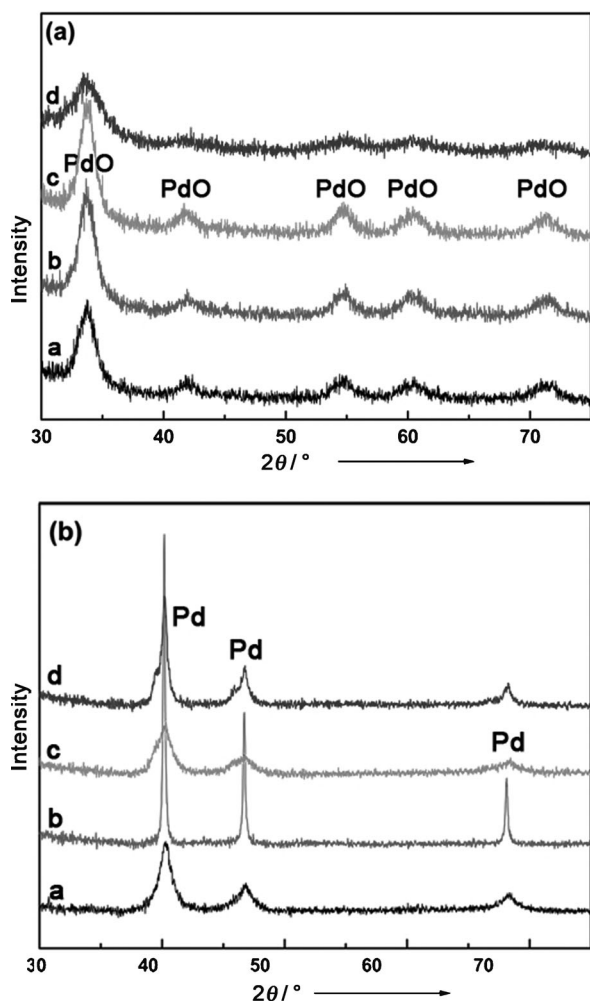


Figure 2. XRD patterns of catalysts [a: Pd/SiO₂(ME), b: Pd/SiO₂(Imp), c: Pd-MgO/SiO₂(ME), d: Pd-MgO/SiO₂(Imp)] (a) as-synthesized catalysts and (b) after reaction.

and H₂ production of Pd/SiO₂(ME) decreased more than 35% after 15 h of reaction. Because the SiO₂ encapsulant effectively prevents agglomeration of the Pd nanoparticles in the Pd/SiO₂(ME) (see Figure S3 in the Supporting Information for TEM images), we postulate that coking or other kinetic issues are responsible for Pd/SiO₂(ME) deactivation.

Remarkably, MgO addition to Pd/SiO₂(ME) and Pd/SiO₂(Imp) completely prevents rapid deactivation; catalysts with MgO consistently produce more CO and H₂ than their MgO-free counterparts. Given that MgO does not physically prevent Pd agglomeration (Figure 1 b and d), we propose that MgO either chemically prevents carbon deposition on Pd by removing the carbon intermediate from Pd or it creates additional fast reaction pathways. The MgO modifier also increases the amount of initial CO and H₂ production of Pd-MgO/SiO₂(Imp) by approximately 80% over MgO-free Pd/SiO₂(Imp). We are, therefore, confident of the critical role that MgO plays in catalytic activity and resistance to catalyst deactivation.

Despite high initial CO and H₂ production, the activity of Pd-MgO/SiO₂(Imp) gradually decreases by as much as 10% due to Pd agglomeration, as shown in Figure 1 b and d, where-

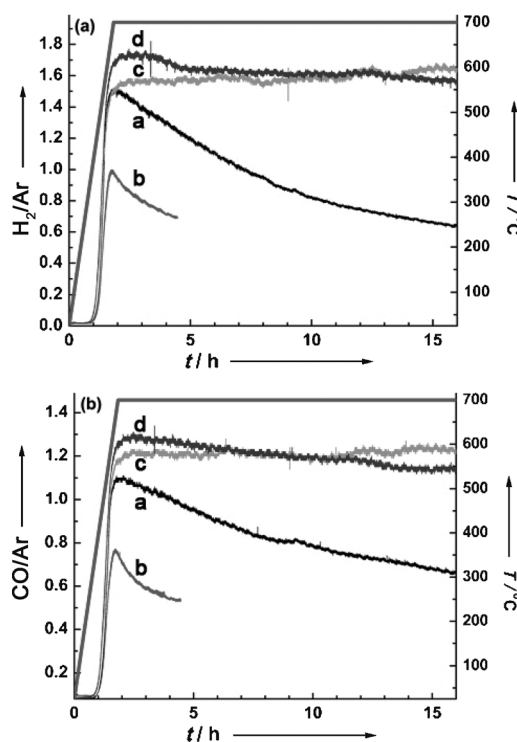


Figure 3. Steady-state CO₂ reforming of CH₄ at 700 °C on the catalysts [a: Pd/SiO₂(ME), b: Pd/SiO₂(Imp), c: Pd-MgO/SiO₂(ME), d: Pd-MgO/SiO₂(Imp)] studied in (a) H₂/Ar and (b) CO/Ar. The straight line shows the temperature profile. Pd-MgO/SiO₂(ME) and Pd-MgO/SiO₂(Imp) were prepared from 6.2 and 3.6 wt% initial Pd and Mg content, respectively.

Table 1. Activities of studied catalysts at various reaction conditions.

Catalyst	T [°C]	TOS ^[a] [h]	CH ₄ conversion [%]	CH ₄ reaction rate [10 ⁻⁶ mol _{cat.} ⁻¹ s ⁻¹]
Pd/SiO ₂ (ME)	450	1	9.6	1.42
	700	1	61.8	9.20
	700	15	31.0	4.61
Pd/SiO ₂ (Imp)	450	1	7.4	1.10
	700	1	46.2	6.88
	700	15	0	0
Pd-MgO/SiO ₂ (ME)	450	1	14.4	2.14
	700	1	64.5	9.60
	700	15	65	9.67
Pd-MgO/SiO ₂ (Imp)	450	1	12.2	1.82
	700	1	65.7	9.78
	700	15	63.5	9.45

[a] TOS = time on stream.

as that of Pd-MgO/SiO₂(ME) is constant over 15 h without any deactivation. Such excellent sinter resistance of Pd-MgO/SiO₂(ME) at high temperatures would assure stable catalytic activity and catalyst renewability when applied under industrial conditions.

Thermogravimetric analysis results on used catalysts give credence to the novelty of the ME method and the essential role of MgO in coking resistance. The catalysts synthesized by

the reverse ME method, Pd–MgO/SiO₂(ME) and Pd/SiO₂(ME), show a minimal mass loss, indicating low residual carbon content on these catalysts, which represents their excellent coking resistance (see Figure S4 in the Supporting Information). Temperature-programmed oxidation (TPO) studies on used catalysts confirmed CO₂ formation and that oxidation of the deposited coke onto the catalyst surface was responsible for the mass loss (see Figure S5 in the Supporting Information). Coke resistance of encapsulated nanoparticles has been generally observed, but is not fully understood.^[18,19] We hypothesize that the structural framework and/or specific contact area between a Pd nanoparticle and the porous SiO₂ encapsulant is likely to protect Pd from PdC formation.^[18] Because Pd–MgO/SiO₂(Imp) showed significantly reduced fractional mass loss compared with Pd/SiO₂(Imp), we conclude that the MgO additive enhances the coking resistance of Pd. Notably, Pd/SiO₂(ME), with a rapid drop in catalytic activity (Figure 3), shows an extremely low mass loss and low CO₂ emission during the TPO experiment. These findings suggest that deactivation of Pd/SiO₂(ME) is due to kinetic issues, such as competition between the reactants for the single adsorption site, or poisoning rather than coking. This reconfirms the critical effects of MgO upon the reaction mechanism and kinetics.

A comparative study of Pd/SiO₂(ME), MgO/SiO₂(ME), and Pd–MgO/SiO₂(ME) at low temperature demonstrates the synergistic interplay of MgO and Pd (Figure 4 and Figure S6 in the Supporting Information). The catalysts without Pd or MgO are not highly reactive, indicating that Pd and MgO work together to achieve the superior catalytic activity of Pd–MgO/SiO₂(ME). Remarkably, the effects of MgO were saturated at a very low MgO content (2.3 wt% of the initial Mg loading, Figure 4).

We therefore hypothesize that MgO preferentially segregates to the interface between Pd and SiO₂, forming the Pd–MgO contact (rather than mixing with porous SiO₂); such a Pd–MgO interface is where the synergy of Pd and MgO originates. Therefore, we propose a three-layer structure, a Pd nanoparticle core covered with a thin porous MgO layer and a porous SiO₂ shell, as shown in Figure 5. The H₂-TPR profile for Pd–MgO/SiO₂(ME) is broader than that of Pd/SiO₂(ME); this shows that dispersed PdO is in contact with MgO due to the strong interactions of PdO and MgO (see Figure S7 in the Supporting Information for details of the H₂-TPR results).

DFT studies on the multifunctional CH₄ reforming mechanism

When experiments are not able to provide mechanistic information regarding the reaction and the role of individual components, computational methods such as DFT are very valuable. DFT studies on catalysis by metallic surfaces of nanoparticles and oxides have reinforced critical information in designing and validating nanocatalysts.^[20] To the best of our knowledge, however, there are few computational studies on bifunctional catalysts (less than 30 articles on bifunctional catalysis in Web of Science). Most research has focused on a specific feature of the catalyst or dealt with the bifunctional mechanism of a single-element catalyst.

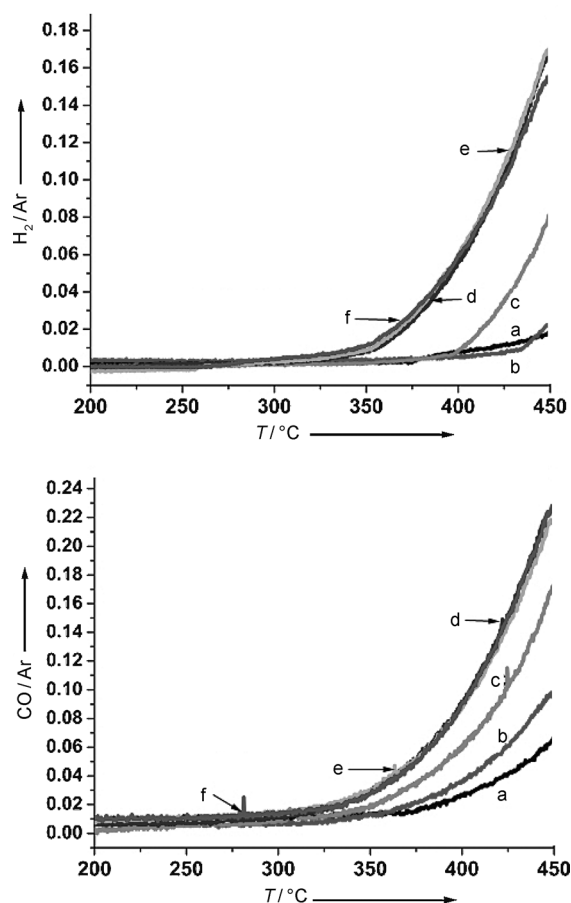


Figure 4. Effect of Mg loading [a: 0.0 (Pd/SiO₂), b: 0.5, c: 1.1, d: 2.3, e: 3.6, f: 6.8 wt%] on H₂ (top) and CO (bottom) production of Pd–MgO/SiO₂(ME) catalyst. H₂ and CO production is saturated at an Mg loading of 2.3 wt%.

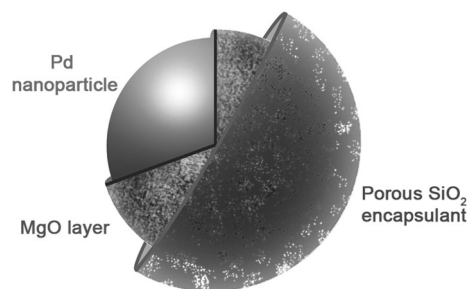


Figure 5. Schematic structure of Pd–MgO/SiO₂(ME)

Despite experimental and theoretical studies on SR and DR of CH₄ catalyzed by transition-metal catalysts, their reaction mechanism and reaction intermediates are still under debate.^[21–24] Maestri et al. indicated that when CH₄ was completely dissociated into C' and 4H' (CH₄ → C' + 4H') by a Rh catalyst, the hydroxyl radical (OH') oxidized C' of CH₄ (OH' + C' → CO' + H').^[22] They further reported that the OH' was supplied by H₂O dissociation (H₂O → OH' + H') or CO₂ activation with H' (CO₂ + H' → CO' + OH') for SR or DR of CH₄ reforming, respectively. In the case of SR of CH₄, van Grootel et al. pointed out that CH₄ did not completely dissociate into C' and 4H' on a Rh

catalyst.^[23] Rather, the CH^{*} intermediate participates in the formation of CHO^{*}, which subsequently dissociates into CO^{*} and H^{*}.^[23] Additionally, in their study on the activity of several transition-metal catalysts for the SR of CH₄, Nørskov and co-workers^[21] and Yamaguchi and Iglesia^[24] found that metal catalysts completely dissociated CH₄ and H₂O, whereby CO and H₂ were produced through the subsequent association of C^{*}, H^{*}, and O^{*}.

Aiming to provide insight into the cooperative role of MgO and Pd with regard to CH₄ reforming, we have designed a Pd–MgO interface, studied the reaction mechanism, and calculated the CH₄ binding energies and subsequent dissociation on Pd, and CO₂ adsorption on MgO, to generate initial reacting species. Results in Figure 6a (details on energetics of CH₄ adsorption and dissociation and corresponding geometries are presented in Table S2 and Figure S8 in the Supporting Information) show that MgO strongly binds CO₂ while Pd binds and completely dissociates CH₄ into Pd–C^{*} and Pd–H^{*}. Results of temperature-programmed desorption of CO₂ also prove that MgO binds CO₂ (Figure S9 in the Supporting Information). After such initial steps, Pd–C^{*}, Pd–H^{*}, and MgO–CO₂^{*} are generated as reaction intermediates.

Figure 6a shows the simplest reaction pathway that can directly produce CO. Detailed reaction pathways are presented in Figure S10 in the Supporting Information. To produce CO from MgO–CO₂^{*}, the only oxygen source in the system, the energetics of MgO–CO₂^{*} dissociation were examined by transferring one oxygen atom from MgO–CO₂^{*} to two possible candidates: Pd and Pd–C^{*}. We found that oxygen transfer from MgO–CO₂^{*} to a Pd nanoparticle (MgO–CO₂^{*} → MgO–CO^{*} + Pd–O^{*}) or Pd–C^{*} (MgO–CO₂^{*} → MgO–CO^{*} + Pd–CO^{*}) requires 2.89 and 0.95 eV, respectively. Formation of the Pd–CO^{*} species is, therefore, more favorable than Pd–O^{*}, and Pd–C^{*} supplied

from CH₄ dissociation acts as an oxygen acceptor. By transferring one oxygen atom from the MgO–CO₂^{*} intermediate to Pd–C^{*}, Pd–CO^{*} and MgO–CO^{*} are generated. As the energy of atomic oxygen transfer is highly dependent on the position of Pd–C^{*} on Pd, the energy of the reaction and the activation energy are likely to be sensitive to the thermal diffusivity of the reactant species on the catalyst surfaces.

Notably, the energy of CO desorption from MgO–CO^{*} (+0.60 eV) is much lower than that from Pd–CO^{*} (+1.99 eV, not shown in Figure 6 for brevity). The entropic contribution to the Gibbs free energy change upon CO desorption, which could lower the energy needed for CO desorption, is roughly –0.61 eV at 25 °C [standard entropy of CO(g) is 197.67 J mol^{–1} K^{–1}].^[25] Therefore, a large fraction of CO comes from MgO–CO^{*}. Moreover, moving adsorbed CO^{*} from Pd–CO^{*} to MgO is more energetically favorable than direct CO desorption from Pd–CO^{*}. At sufficiently high temperatures, residual CO in the Pd nanoparticles (Pd–CO^{*}) preferentially moves to MgO (CO spillover, +1.39 eV) first and is desorbed later. As such, MgO supports an alternative two-step pathway for CO desorption from Pd–CO^{*}, with CO produced from two different carbon sources, CO₂ and CH₄. This finding gives credence to our experimental statement that MgO enhances coking resistance of Pd by removing the carbon species from Pd. Because MgO facilitates CO production and helps Pd to access other reaction species by removing CO from Pd, MgO essentially also increases the catalytic activity.

Interestingly, from the early stages of the reaction, low amounts of H₂O were consistently produced (Figure 7). In this case, side reactions such as hydrogen transfer from Pd–H^{*} to MgO–CO₂^{*} or a reverse water gas shift reaction are probably responsible for spontaneous H₂O production. We found that H

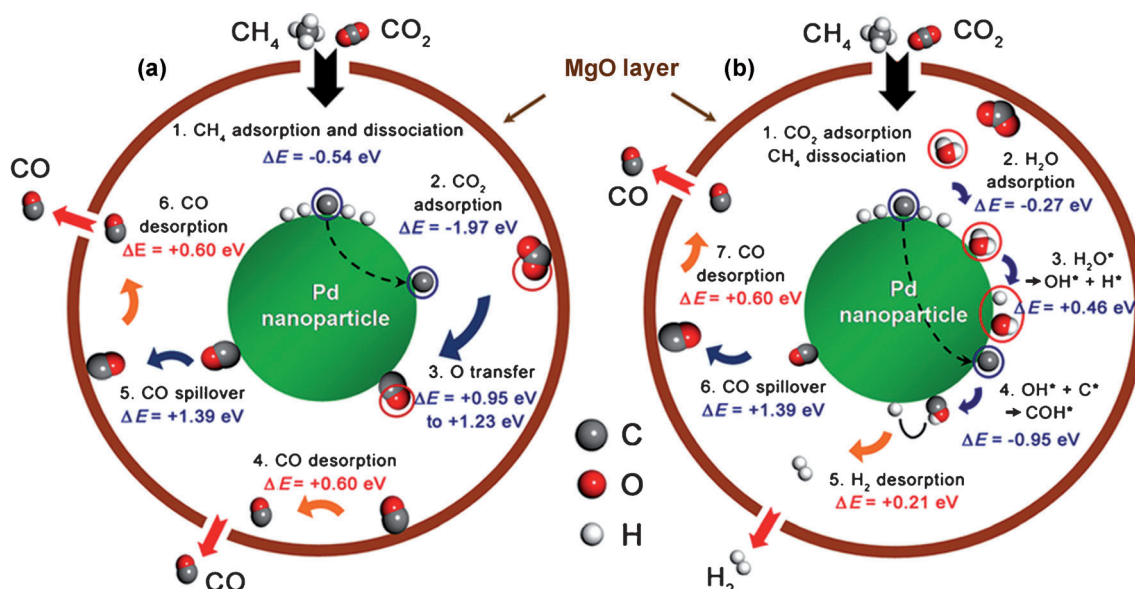


Figure 6. Results from DFT studies on the multifunctional CH₄ reforming mechanism under dry reforming conditions (a) and an H₂O atmosphere (b). The reaction proceeds in clockwise direction. Pd dissociates CH₄ and MgO binds and activates CO₂. MgO opens a favorable CO production pathway. H₂O byproducts are attributed to H₂ production. Pd dissociates H₂O into Pd–OH^{*} and Pd–H^{*}. Pd–OH^{*} and Pd–C^{*} were combined into Pd–COH^{*}. H₂ association from Pd–COH^{*} and Pd–H^{*} is easier than direct H₂ association from two Pd–H^{*}. These CO and H₂ production pathways are accessible at low temperature and assure low-temperature activity of Pd–MgO/SiO₂(ME).

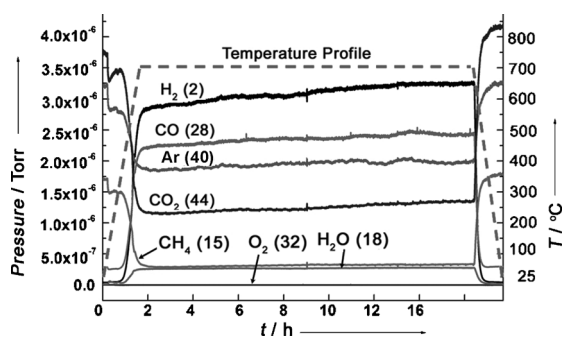


Figure 7. Steady-state CO₂ reforming of CH₄ at 700 °C on Pd-MgO/SiO₂(ME). The production of CO, H₂, and H₂O during the reaction is observed by mass spectrometry. The Mg loading of Pd-MgO/SiO₂(ME) was 3.6 wt %.

transfer from Pd-H* to MgO-CO₂* was an endothermic process by 1.52 eV. This energy is not too high compared with other endothermic steps, for example, CO spillover requires 1.39 eV. Thus, small amounts of water can be produced. On the other hand, H transfer from Pd-H* to MgO-CO₂* requires more energy than O transfer from MgO-CO₂* to Pd-C* (step 3 in Figure 6a) and the energy of H transfer is also higher than the energy of direct H₂ desorption from two Pd-H* pairs (1.25 eV), confirming why CO and H₂, rather than H₂O, are the main products of the reaction.

Because the participation of H₂O in CH₄ reforming is an essential step for the SR of CH₄, we have additionally studied the SR of CH₄ on the present model catalyst. Figure 6b and Figure S11 in the Supporting Information show another reaction pathway that can be activated under an H₂O atmosphere (SR of CH₄). Pd can bind H₂O and dissociate into Pd-OH* and Pd-H*.

Yamaguchi and Iglesia reported the further dissociation of Pd-OH* into Pd-O* and Pd-H*.^[24] However, we found the association of Pd-OH* and Pd-C* to Pd-COH* was highly favorable (-0.99 eV). Moreover, direct CO desorption from Pd-COH* (Pd-COH* → Pd-H* + CO(gas), ΔE = +0.95 eV) is easier than direct CO desorption from Pd-CO* (+1.99 eV). Therefore, CO desorption from Pd-COH*, as well as CO desorption from MgO-CO* and two-step CO desorption through CO spillover, may contribute together to the total CO production. Nevertheless, the most important role of the Pd-COH* intermediate is its contribution to H₂ production. In fact, because Pd dissociates H₂ readily and binds H strongly, desorption of H₂ from two Pd-H* requires a lot of energy (+1.25 eV). Conversely, in the presence of Pd-COH*, it is relatively easy to remove H₂ from Pd-COH* and Pd-H* (+0.21 eV). Residual CO on Pd (Pd-CO*) can spillover onto MgO and be desorbed as described in Figure 6a and b. Eventually, although we supplied the mixture of CO₂ and CH₄, which are the typical reactants for the DR of CH₄, H₂O was spontaneously formed in the very first stage of the reaction, and thus, the SR of CH₄ operated simultaneously. Because the present findings indicate that H₂O produced as a byproduct can contribute to the reaction process, we thus maintain that both the DR and SR of CH₄ need to be considered altogether when one designs and validates new catalysts for CH₄ reforming.

Novelty of the Pd-MgO/SiO₂(ME) catalyst

To utilize abundant CH₄ and CO₂ efficiently, low-temperature CH₄ reforming is a promising route because this reaction can be combined with CO hydrogenation to produce hydrocarbon chemicals at low temperatures. Since the direct production of hydrocarbon chemicals can be catalyzed by using physically mixed or a double-layer catalyst (low-temperature CH₄ reforming catalyst + FT synthesis catalyst), the reaction of CH₄ and CO₂ at low temperatures to form syngas, followed by subsequent conversion through FT synthesis into fuels, is an attractive route for the utilization of both chemicals.

Table 1 shows that the present Pd-MgO/SiO₂(ME) catalyst clearly produces CO and H₂ in a lower temperature region. The start-of-reaction temperature of Pd-MgO/SiO₂(ME) is around 300 °C (see Figure 4), which is at least 100 °C lower than Ni-based transition-metal-modified catalysts already reported as catalysts reactive at low temperature.^[9] Analysis of low-temperature CH₄ reforming over Pd-MgO/SiO₂(ME) and Ni/SiO₂(Imp) catalysts indicates that Pd-MgO/SiO₂(ME) shows a better low-temperature activity than the conventional Ni-based catalyst (see Figure S12 in the Supporting Information).

We propose the modification of a metal catalyst with the addition of MgO as a promising strategy in designing a low-temperature catalyst for syngas production and suggest that Pd-MgO/SiO₂(ME) described herein is better suited for in situ fuel and hydrocarbon production by FT synthesis than traditional transition-metal catalysts.

The CH₄ conversion rate of our Pd-MgO/SiO₂(ME) catalyst at 700 °C (65%) is comparable with the reported CH₄ conversion rate of a ZrO₂-modified Ni catalyst with a BET surface area of 180.9 cm²g⁻¹ (63%). Tomiyama et al. reported carbon deposition around of 0.01 g g_{cat}⁻¹ after a 4 h activity test on their Ni-based catalysts.^[13] The amount of carbon deposition in Pd-MgO/SiO₂(ME) after 15 h at 700 °C is negligibly small (see Figure S5 in the Supporting Information). These results confirm the superior coking and sintering resistance of Pd-MgO/SiO₂(ME) due to the multifunctional mechanism of CH₄ reforming.

Conclusions

Herein, we combined state-of-the-art, one-pot, in situ reverse microemulsion (ME) synthesis and an understanding of a multifunctional reaction mechanism from DFT to suggest a substantial strategy to design novel catalysts for CH₄ reforming. Experimental analysis and the first DFT study on multifunctional catalysis revealed the excellent properties of the Pd-MgO/SiO₂(ME) catalyst. A unique and groundbreaking feature of the present catalyst is the well-designed cooperation of each element that assures long-lasting stability, low-temperature activity, and consistently high activity. We thus suggest the one-pot ME method as a method to synthesize highly dispersed composite catalysts for complicated chemical reactions. The present SiO₂-encapsulated, oxide-modified, metal catalyst model would be a new standard of multistep heterogeneous catalysts as green chemistry accompanies high stability and activity.

Experimental Section

Catalyst preparation: To investigate the effects of the SiO₂ shell and MgO content on the catalytic properties, we synthesized Pd–MgO/SiO₂(ME) catalysts with various initial Mg loadings (0–6.8 wt%) by a reverse ME method, and two control group catalysts (Pd/SiO₂(Imp) and Pd–MgO/SiO₂(Imp)) by a conventional impregnation method.

The Pd–MgO/SiO₂(ME) catalyst was synthesized from reverse ME by adding an aqueous mixture of Pd(NO₃)₂·H₂O (Aldrich, 7 mL, 0.028 M) and Mg(NO₃)₂·6H₂O (Aldrich, 3 mL, 0.169 M) to a vigorously stirred solution containing a nonionic surfactant (40 mL, Igepal CO-520, Aldrich) and cyclohexane (100 mL, Fisher Scientific).^[16] During stirring, hydrazine (64 μL, Aldrich 98%) was added to the mixture, which was stirred for 1 h. An aqueous solution of NH₄OH (EMD, 28%) was then added to adjust the pH to 11. After another hour of stirring, a mixture of tetraethyl orthosilicate (TEOS, 0.995 mL, Acros organic) and *n*-octadecyltrimethoxysilane (C₁₈TMS, 0.357 mL, Gelest) was added dropwise. Hydrolysis and condensation of the silica precursors was allowed to proceed in the stirred mixture for 3 days at 20 °C. After condensation, Pd–MgO/SiO₂(ME) precipitated and was washed with ethanol. The ethanol wash was followed by centrifugation (repeated three times). Pd–MgO/SiO₂(ME) was then dried at 100 °C and calcined at 550 °C in air for 6 h; the heating rate was 1 °C min⁻¹. The Pd loading was 6.2 wt%, and the loading of the second Mg metal varied from 0 to 6.8 wt%. The Pd/SiO₂(ME) catalyst was synthesized by using a palladium nitrate precursor, Pd(NO₃)₂·H₂O (Aldrich, 10 mL, 0.02 M), identical to that described above for Pd–MgO/SiO₂(ME).

For the synthesis of silica impregnated with a Pd catalyst, Pd/SiO₂(Imp) was synthesized on silica spheres produced from a reverse ME process identical to that described above for Pd/SiO₂(ME), with the Pd precursor replaced with an aqueous solution of NH₄OH and without a reducing agent. The SiO₂ spheres (0.35 g) were added to a solution of Pd(NO₃)₂·H₂O (0.05 g) in water (40 mL) and stirred for 4 h at 80 °C, then dried at 110 °C, and calcined at 550 °C in air for 6 h; the heating rate was 1 °C min⁻¹. The Pd–MgO/SiO₂(Imp) catalyst was synthesized by using palladium and magnesium nitrate precursors, Pd(NO₃)₂·H₂O and Mg(NO₃)₂·H₂O, identical to those described above for Pd/SiO₂(Imp).

Catalyst characterization: The catalyst morphology was investigated by TEM (JEN2100F, JEOL), and the elemental distribution monitored by energy-dispersive X-ray spectroscopy (Oxford INCA) with a system integrated to the TEM. To determine the particle size distribution and average particle size, 100 particles from the TEM images were measured. Errors were taken as the standard deviation of the particle sizes. X-ray diffraction was performed on selected samples over the scattering range of $30 \leq 2\theta \leq 75$ with steps of 0.017° by using CuK_α radiation (Philips X'Pert Pro X-ray diffractometer). The BET surface areas and pore volumes were estimated by using the N₂ adsorption–desorption isotherms (Micromeritics, Model ASAP 2400). Temperature-programmed reduction with H₂ (H₂-TPR) and CO₂ temperature-programmed desorption (CO₂-TPD) were performed by using a fixed-bed flow system connected to a thermal conductivity detector (TCD). For H₂-TPR, samples (30 mg) were pretreated in O₂ at 500 °C for 1 h and He at 500 °C for 30 min, cooled to room temperature, and then samples were exposed to 10% H₂ in He while increasing the temperature from 25 to 900 °C at a rate of 10 °C min⁻¹. In CO₂-TPD, the catalysts (30 mg) were first pretreated at 400 °C for 1 h with He, cooled to room temperature, exposed to 100% CO₂ flow (30 mL min⁻¹) for 1 h, purged in He for 1 h, and then the desorption temperature was increased linearly to 900 °C at 10 °C min⁻¹. During this programmed temperature opera-

tion, H₂-TPR and CO₂-TPD patterns were measured by the TCD. To characterize the catalysts after reactions, thermogravimetric (TG)/temperature-programmed oxidation (TPO) and TPO analysis were performed after CH₄ reforming at 700 °C for 15 h. Both TG/TPO and TPO analysis was done in 50% O₂ in N₂. We used the Mettler STARe Thermo Gravimetric Analyzer (TGA/sDTA851e) for TG/TPO analysis and a fixed-bed reactor system connected to a mass spectrometer (RGA) for TPO analysis with a flow rate of 50 mL min⁻¹. The temperature was increased to 800 °C at a rate of 10 °C min⁻¹ for TGA/TPO and TPO analysis.

Catalytic activity run: The catalytic test for CO₂ reforming of CH₄ was carried out in an atmospheric-pressure fixed-bed reactor with an inner diameter of 6 mm in the range of 25–700 °C. A reaction gas mixture ratio of CO₂/CH₄/Ar was 1/1/1.5. The amount of catalyst was 0.1 g (40–60 mesh particle size) and space time was 1.1 s. Before the reaction, the catalyst was pretreated at 450 °C for 1 h in 10 wt% H₂ in an Ar flow. The reactants (CO₂, CH₄, and Ar) and products (H₂ and CO) were analyzed on a gas chromatograph (SRI) connected to a 5 Å molecular sieve column and mass spectrometer (RGA) at the same time. For temperature-programmed CO₂ reforming of CH₄ the heating rate was 7.5 °C min⁻¹. To record the activity at different reaction temperatures, the CO₂ reforming of CH₄ was performed for 1 h at every reaction temperature.

Theoretical predictions: We designed a simplified slab model that could describe an interface between Pd and MgO. Through the introduction of a bifacial linear Pd structure (linear nanoparticle with 24 atoms), a Pd(111) surface area wider than the supported spherical or faceted nanoparticles was assured (Figure S13 in the Supporting Information). A Pd nanoparticle was supported on the MgO(110) surface and fully optimized to produce an interface between Pd and MgO. We contend that, under the current level of computational power, this is the most efficient model to study a complicated reaction mechanism involving various reaction intermediates.

Spin-polarized Kohn–Sham DFT calculations were executed with the plane-wave VASP code^[26] and the RPBE^[27] GGA functional. The plane wave energy cutoff was 290 eV. The ionic cores were described by the projector-augmented wave method implemented in the Vienna ab initio simulation package.^[26] We employed a 4×5 MgO(110) slab with six atomic layers and a 20 Å vacuum thickness. Due to the large size of the system, a gamma point sampling of the Brillouin zone for all calculations was used. The final convergence criteria for the electronic wave function and for the geometry were 10⁻⁴ eV and 0.01 eV Å⁻¹, respectively. We used the Gaussian smearing method with a window size of 0.1 eV to improve convergence with respect to states near the Fermi level.

Acknowledgements

H.Y.K. is supported by the Department of Energy under contract DE-SC0001091 and his calculations were performed at the National Energy Research Scientific Computing Center. J.N.P. thanks Prof. Eric W. McFarland (UCSB) for useful discussions and support. J.N.P. and J.M.K. thank the Priority Research Centers program (20011-0031392) and the WCU (World Class University, R31-2008-10029) program through the National Research Foundation of Korea. H.Y.K. was partially supported by National Research Foundation of Korea Grant funded by the Korean Government (Ministry of Education, Science and Technology; NRF-2011-357-D00118).

Keywords: density functional calculations · green chemistry · heterogeneous catalysis · methane · nanostructures

- [1] a) J. F. B. Mitchell, T. C. Johns, J. M. Gregory, S. F. B. Tett, *Nature* **1995**, 376, 501–504; b) J. R. Petit, J. Jouzel, D. Raynaud, N. I. Barkov, J.-M. Barnola, I. Basile, M. Bender, J. Chappellaz, M. Davis, G. Delaygue, M. Delmotte, V. M. Kotlyakov, M. Legrand, V. Y. Lipenkov, C. Lorius, L. Pépin, C. Ritz, E. Saltzman, M. Stievenard, *Nature* **1999**, 399, 429–436; c) C. D. Thomas, A. Cameron, R. E. Green, M. Bakkenes, L. J. Beaumont, Y. C. Collingham, B. F. N. Erasmus, M. Ferreira de Siqueira, A. Grainger, L. Hannah, L. Hughes, B. Huntley, A. S. van Jaarsveld, G. F. Midgley, L. Miles, M. A. Ortega-Huerta, A. T. Peterson, O. L. Phillips, S. E. Williams, *Nature* **2004**, 427, 145–148.
- [2] H. J. Smith, J. Fahrenkamp-Uppenbrink, R. Coontz, *Science* **2009**, 325, 1641–1641.
- [3] D. T. Whipple, P. J. A. Kenis, *J. Phys. Chem. Lett.* **2010**, 1, 3451–3458.
- [4] a) S. Chu, *Science* **2009**, 325, 1599–1599; b) R. S. Haszeldine, *Science* **2009**, 325, 1647–1652; c) D. W. Keith, *Science* **2009**, 325, 1654–1655; d) G. T. Rochelle, *Science* **2009**, 325, 1652–1654.
- [5] S. E. Park, J. S. Yoo in *Carbon Dioxide Utilization for Global Sustainability*, Vol. 153 (Eds.: S. E. Park, J. S. Chang, K. W. Lee), Elsevier, Amsterdam, **2004**, pp. 303–314.
- [6] M. C. J. Bradford, M. A. Vannice, *Catal. Rev.* **1999**, 41, 1–42.
- [7] M. S. Fan, A. Z. Abdullah, S. Bhatia, *ChemCatChem* **2009**, 1, 192–208.
- [8] a) J. R. Rostrupnielsen, J. H. B. Hansen, *J. Catal.* **1993**, 144, 38–49; b) D. A. Hickman, L. D. Schmidt, *Science* **1993**, 259, 343–346.
- [9] T. V. Choudhary, V. R. Choudhary, *Angew. Chem.* **2008**, 120, 1852–1872; *Angew. Chem. Int. Ed.* **2008**, 47, 1828–1847.
- [10] a) C. S. Chen, S. J. Feng, S. Ran, D. C. Zhu, W. Liu, H. J. M. Bouwmeester, *Angew. Chem.* **2003**, 115, 5354–5356; *Angew. Chem. Int. Ed.* **2003**, 42, 5196–5198; b) A. T. Ashcroft, A. K. Cheetham, M. L. H. Green, P. D. F. Vernon, *Nature* **1991**, 352, 225–226; c) A. T. Ashcroft, A. K. Cheetham, J. S. Foord, M. L. H. Green, C. P. Grey, A. J. Murrell, P. D. F. Vernon, *Nature* **1990**, 344, 319–321; d) V. R. Choudhary, K. C. Mondal, A. S. Mamman, *J. Catal.* **2005**, 233, 36–40; e) F. Besenbacher, I. Chorkendorff, B. S. Clausen, B. Hammer, A. M. Molenbroek, J. K. Nørskov, I. Stensgaard, *Science* **1998**, 279, 1913–1915; f) H. S. Bengaard, J. K. Nørskov, J. Sehested, B. S. Clausen, L. P. Nielsen, A. M. Molenbroek, J. R. Rostrup-Nielsen, *J. Catal.* **2002**, 209, 365–384; g) F. Basile, P. Benito, P. Del Gallo, G. Fornasari, D. Gary, V. Rosetti, E. Scavetta, D. Tonelli, A. Vaccari, *Chem. Commun.* **2008**, 2917–2919.
- [11] J. H. Bitter, K. Seshan, J. A. Lercher, *J. Catal.* **1999**, 183, 336–343.
- [12] a) J. H. Bitter, K. Seshan, J. A. Lercher, *J. Catal.* **1998**, 176, 93–101; b) S. Menad, P. Ferreira-Aparicio, O. Cherifi, A. Guerrero-Ruiz, I. Rodriguez-Ramos, *Catal. Lett.* **2003**, 89, 63–67; c) S. Therdthianwong, C. Siangchin, A. Therdthianwong, *Fuel Process. Technol.* **2008**, 89, 160–168.
- [13] S. Tomiyama, R. Takahashi, S. Sato, T. Sodesawa, S. Yoshida, *Appl. Catal. A: Gen.* **2003**, 241, 349–361.
- [14] a) T. I. Doukov, T. M. Iverson, J. Seravalli, S. W. Ragsdale, C. L. Drennan, *Science* **2002**, 298, 567–572; b) M. Yamakawa, H. Ito, R. Noyori, *J. Am. Chem. Soc.* **2000**, 122, 1466–1478; c) K. G. Azzam, I. V. Babich, K. Seshan, L. Lefferts, *J. Catal.* **2007**, 251, 153–162; d) J. B. Park, J. Graciani, J. Evans, D. Stacchiola, S. D. Senanayake, L. Barrio, P. Liu, J. F. Sanz, J. Hrbek, J. A. Rodriguez, *J. Am. Chem. Soc.* **2010**, 132, 356–363.
- [15] H. Y. Kim, H. M. Lee, J.-N. Park, *J. Phys. Chem. C* **2010**, 114, 7128–7131.
- [16] J.-N. Park, E. W. McFarland, *J. Catal.* **2009**, 266, 92–97.
- [17] J.-N. Park, A. J. Forman, W. Tang, J. H. Cheng, Y. S. Hu, H. F. Lin, E. W. McFarland, *Small* **2008**, 4, 1694–1697.
- [18] A. J. Forman, J.-N. Park, W. Tang, Y. S. Hu, G. D. Stucky, E. W. McFarland, *ChemCatChem* **2010**, 2, 1318–1324.
- [19] S. Takenaka, Y. Orita, H. Umabayashi, H. Matsune, M. Kishida, *Appl. Catal. A: Gen.* **2008**, 351, 189–194.
- [20] a) J. K. Nørskov, T. Bligaard, J. Rossmeisl, C. H. Christensen, *Nat. Chem.* **2009**, 1, 37–46; b) H. Falsig, B. Hvolbaek, I. S. Kristensen, T. Jiang, T. Bligaard, C. H. Christensen, J. K. Nørskov, *Angew. Chem.* **2008**, 120, 4913–4917; *Angew. Chem. Int. Ed.* **2008**, 47, 4835–4839; c) H. Y. Kim, H. M. Lee, R. G. S. Pala, V. Shapovalov, H. Metiu, *J. Phys. Chem. C* **2008**, 112, 12398–12408.
- [21] G. Jones, J. Geest Jakobsen, S. S. Shim, J. Kleis, M. P. Andersson, J. Rossmeisl, F. Abild-Pedersen, T. Bligaard, S. Helveg, B. Hinnemann, J. R. Rostrup-Nielsen, I. Chorkendorff, J. Sehested, J. K. Nørskov, *J. Catal.* **2008**, 259, 147–160.
- [22] M. Maestri, D. G. Vlachos, A. Beretta, G. Groppi, E. Tronconi, *J. Catal.* **2008**, 259, 211–222.
- [23] P. W. van Grootel, E. J. M. Hensen, R. A. van Santen, *Langmuir* **2010**, 26, 16339–16348.
- [24] A. Yamaguchi, E. Iglesia, *J. Catal.* **2010**, 274, 52–63.
- [25] P. Atkins, J. D. Paula, *Physical Chemistry*, 8th ed., Oxford, New York, **2006**.
- [26] a) G. Kresse, J. Furthmüller, *Comput. Mater. Sci.* **1996**, 6, 15–50; b) G. Kresse, J. Furthmüller, *Phys. Rev. B* **1996**, 54, 11169–11186.
- [27] B. Hammer, L. B. Hansen, J. K. Nørskov, *Phys. Rev. B* **1999**, 59, 7413–7421.

Received: December 6, 2011

Revised: January 28, 2012

Published online on June 15, 2012